A Combined Solid-State NMR and Diffraction Study of the Structures and Acidity of Fluorinated Aluminas: Implications for Catalysis

Peter J. Chupas,[†] David R. Corbin,[‡] V. N. M. Rao,[‡] Jonathan C. Hanson,[§] and Clare P. Grey*[,†]

Department of Chemistry, State University of New York at Stony Brook, Stony Brook, New York 11794-3400, DuPont Central Research and Development, Wilmington, Delaware 19880-0262, and Chemistry Department, Brookhaven National Laboratory, Upton, New York 11973

Received: January 23, 2003

We have investigated the structures of a series of pristine and Zn^{2+}-impregnated aluminas following fluorination with HF, by using both solid-state NMR and X-ray powder diffraction methods. In the absence of any cation impregnation, α-AlF_3 and small amounts of β-AlF_3 are formed at a temperature of 400 °C with an HF/N_2 ratio of 1/1. Even higher fractions of β-AlF_3 are formed from the impregnated phases for HF levels of 30% and higher, along with a significant concentration of α-AlF_3. In contrast, fluorination of Zn^{2+}-impregnated γ-Al_2O_3 in dilute HF feeds resulted in formation of the aluminum (hydroxy)fluoride pyrochlore phase, AlF_2-OH, in significant quantities. Thus, even very low levels of transition metals (<2 wt %) appear to play an important role in controlling the phase formed during the fluorination reaction. The formation of the metastable β-AlF_3 and pyrochlore phases, which both contain three- and six-membered Al rings, is ascribed to the presence of high concentrations of protons, either in the starting material or in the fluorinating agent. The pyrochlore phase is stabilized in the presence of Zn, presumably due to the vacant A site in this structure, which can accommodate Zn^{2+} ions more readily than the vacancies in the β-AlF_3 structure. Basic probe molecules (dimethylphenylphosphine), in combination with ^{31}P NMR, were used to study and quantify the surface acidic sites that are formed as a result of fluorination. On the basis of our work, we suggest that the Zn^{2+} ions are not directly implicated as catalytically active centers. The presence of Zn causes an associated increase in the concentration of coordinatively unsaturated aluminum sites, which can then act as the catalytically active centers for F/Cl exchange reactions.

Introduction

Fluorinated aluminas have found widespread applications as catalysts in the production of hydrochlorofluorocarbons (HCFCs) and hydrofluorocarbons (HFCs)[1−5] and in acid catalysis. The catalytically active fluoriated aluminas have been prepared by a variety of methods, which include gas-phase fluorination with fluorine gas,[6] hydrofluoric acid,[5,7] HFCs,[8] or HCFCs[9−14] and aqueous impregnation with ammonium fluoride.[15−18] Amorphous phases,[11] aluminum hydroxyfluorides,[3,6,12] and different aluminum fluoride phases[7−10,12−14] have all been identified following fluorination. An alternative approach for altering the catalytic properties and the structure of these materials involves the impregnation of the alumina starting materials with transition metals such as Zn^{2+} and Co^{2+}. For example, this approach has been shown to result in increased activities for the HF halogen exchange or addition reactions of CF_3CHCl_2 (HFC-123),[2] CCl_2-CCl_2 (PCE),[3] CF_3CH_2Cl (HFC-133a),[4] and CCl_2CHCl (TCE).[5] The catalytic results from the patent literature are summarized in Table 1. In the zinc-impregnated systems, the catalytic activity was shown to be optimized for Zn loading levels of 2−4%, with higher loading levels often resulting in reduced catalytic activity.

Previous studies of fluorinated alumina have used solid-state NMR,[9,10,15] powder X-ray diffraction (XRD),[6−10] infrared spectroscopy,[11] X-ray photoelectron spectroscopy (XPS),[9,12,13] and/or temperature-programmed desorption (TPD)[13] to study surface and bulk structures and the acid properties of the materials before and after fluorination. For example, Saniger et al. recently reported that γ-Al_2O_3 fluorinated at ambient temperature by fluorine gas yields the pyrochlore phase.[6] Skapin and Kemnitz reported that the fluorination of γ-Al_2O_3 aerogels and xerogels with HF (diluted to 20% in N_2) and CF_3H yielded mixtures of α-AlF_3, β-AlF_3, and AlF_3 hydrates.[7] Three different fluorine sites corresponding to the three aluminum local environments $AlO_{6-x}F_x$ ($x = 1-3$) were identified in a recent solid-state NMR study of fluorinated alumina, prepared through aqueous impregnation with NH_4F. Surprisingly, no bulk AlF_3 phases were identified, even at 12% fluorine loading, and no attempt was made to correlate the nature and concentrations of these sites to acidity.[15] In contrast, bulk AlF_3 phases were identified for fluorine loadings of 10% in another NMR study of materials prepared in a similar manner.[9] XRD patterns of these materials revealed the presence of a mixture of α- and β-AlF_3 and an aluminum hydroxyfluoride, AlF_2OH, with the pyrochlore structure.[9] In our earlier paper, we used a combination of in situ XRD and solid-state ^{19}F and ^{27}Al NMR to investigate the fluorination of γ-Al_2O_3 with HCFC-22 ($CHClF_2$). Octahedral AlF_6 and oxyfluoride environments were shown to exist at temperatures lower than 360 °C, bulk AlF_3 forming at higher temperatures.[10]

Despite much work in this field, the role that the different fluorination agents play in directing the structure and controlling

* To whom correspondence should be addressed. Phone: (631) 632-9548. Fax: (631) 632-5731. E-mail: cgrey@sbchem.sunysb.edu.
[†] State University of New York at Stony Brook.
[‡] DuPont Central Research and Development.
[§] Brookhaven National Laboratory.

10.1021/jp0300905 CCC: $25.00
Published on Web 07/26/2003

TABLE 1: Summary of Catalytic Results from the Patent Literature[2−5]

	Chemistries							
	$CF_3CHCl_2 + xHF \rightarrow CF_3CHFCl + CF_3CHF_2$		$CCl_2{=}CCl_2 + xHF \rightarrow CF_3CHCl_2 + CF_3CHFCl + CF_3CHF_2$		$CF_3CH_2Cl + xHF \rightarrow CF_3CH_2F$		$CCl_2{=}CH\,Cl + xHF \rightarrow CF_3CH_2Cl + CF_3CH_2F$	
catalyst % Zn/Al_2O_3	CF_3CHCl_2 conversn[2] (%)	"β-AlF_3 content" from XRD (I_β/I_α)[a]	$CCl_2{=}CCl_2$ conversn[3] (%)	"β-AlF_3 content" from XRD (I_β/I_α)[a]	CF_3CH_2Cl conversn[4] (%)	"β-AlF_3 content" from XRD (I_β/I_α)[a]	$CCl_2{=}CHCl$ conversn[5] (%)	"β-AlF_3 content" from XRD (I_β/I_α)[a]
0	7.1	0.03	6.6	0.09	2.1	0.28	6.8	0.03
1	33.8	0.11	67.4	0.20	14.2	0.23	81.7	0.11
2	43.1	0.22	90.5	0.18	28.8	0.53	89.2	0.11
4	63.2	0.19	64.9	0.16	19.6	0.16	97.9	0.19
10	33.5	0.41	37.8	0.48	14.6	0.48	96.9	0.43

[a] I_β/I_α is the intensity ratio of the reflection at a *d* spacing of approximately 6.0 Å (a reflection unique to β-AlF_3) to the reflection at a *d* spacing of 3.5−3.6 Å (the intensity of which is dominated by a reflection from α-AlF_3) and defines the relative fraction of β-AlF_3 in the sample.

the acidity of the fluorinated surface remains unclear, and many apparent discrepancies remain in the literature. Structural identification is complicated by the rich structural chemistry of the aluminum oxy/hydoxyfluorides. Many different fluorinated phases have now been synthesized, which, in addition to the thermodynamically stable α-AlF_3 phase,[19] include metastable phases,[20−23] hydrates,[24−27] and hydroxyfluorides.[28] Some of these phases are structurally closely related, making their identification difficult, particularly based on the XRD patterns of the poorly crystalline materials often prepared in situ during fluorination. Identification of the bulk and surface species is, however, critical to the understanding of the catalytic properties of these materials, since the change in the coordination environment of aluminum on fluorination and the increased electronegativity of fluorine as a ligand are reported to be responsible for the observed modification of the acidity, and thus catalytic activity, of these materials.[1]

The acidity of fluorinated aluminas has been studied by the conventional methods TPD and IR. These methods, although widely applied, can leave uncertainties pertaining to the quantification of the number and types of sites and the determination of their relative strength. NMR has not been used in this field to study acidity. However, the use of phosphines as basic probe molecules, in combination with ^{31}P NMR, has been shown to be a valuable tool in the study of acidity, particularly for zeolite solid acids.[33,34] Distinct ^{31}P shifts are seen for phosphines absorbed on solid acid sites, allowing the unambiguous discrimination and quantification of the Brönsted and Lewis acid sites.

In the work reported in this paper, we examine the effect of zinc impregnation of the alumina starting material on the structure and acidity of the fluorinated material. The local and bulk structures are investigated by using a combination of ^{19}F and ^{27}Al MAS and ^{19}F/^{27}Al HETCOR (heteronuclear correlation) NMR spectroscopies and X-ray powder diffraction. The acidities of the surfaces are quantified by sorbing basic phosphine probe molecules and acquiring ^{31}P MAS NMR spectra of the sorbed bases. We show that Zn impregnation alters both the structures formed on fluorination *and* the acidity of the fluorinated material. Dimethylphenylphosphine (DMPP) was used as the probe molecule in this study for two distinct reasons. First, the presence of the phenyl ring increases the size of the molecule relative to the more commonly used probe trimethylphosphine (TMP). This helps to reduce motion and exchange processes on the surface, without significantly increasing the cone angle and subsequent ability to bind to acid sites.[35] Second, dimethylphenylphosphine is less basic than TMP, making it a more suitable probe for highly acidic surfaces and less reactive to phenomena such as dismutation.[36]

Before a detailed ^{19}F NMR analysis of the fluorinated aluminas was performed, our first challenge was to establish a ^{19}F chemical shift scale for these classes of materials. Since this is traditionally achieved by studying model systems, in the remainder of the Introduction of this paper, we discuss materials with known structures that have already been studied by ^{19}F MAS NMR. In particular, we outline some of the apparent contradictions in this field that have led to some confusion in the assignments of the ^{19}F and ^{27}Al NMR spectra of these materials. On the basis of this survey of the literature, a structural study of the model compound β-$AlF_3{\cdot}3H_2O$ was performed, and the data are presented in the first part of the Results.

Fluorine NMR is particularly sensitive (^{19}F has a 100% natural abundance) and can therefore be used effectively to study dilute fluorine species such as the sites found on surfaces. To date, however, no comprehensive correlations between local environments and ^{19}F chemical shifts have been established, making assignment of the different ^{19}F resonances difficult, particularly for heterogeneous aluminum oxyfluoride environments. Previous assignments of fluorinated aluminas have been made on the basis of model compounds such as AlF_3 and $AlF_3{\cdot}3H_2O$.[10,15] However, one problem with this approach is that the nature of the aluminum coordination environments in $AlF_3{\cdot}3H_2O$ has still not been definitively established. Two polymorphs of $AlF_3{\cdot}3H_2O$ have been identified, which have historically been referred to as α-$AlF_3{\cdot}3H_2O$ and β-$AlF_3{\cdot}3H_2O$.[25−27] The crystallographic structures of these materials, while they themselves have not been refined, are known to be isostructural to α-$FeF_3{\cdot}3H_2O$ and β-$FeF_3{\cdot}3H_2O$, respectively.[29] β-$FeF_3{\cdot}3H_2O$, whose XRD pattern can be indexed with a space group identical to and unit cell parameters similar to those of β-$AlF_3{\cdot}3H_2O$, has corner-sharing chains with iron in an octahedral $FeF_4(H_2O)_2$ environment with interstitial water molecules hydrogen-bonded to terminal fluorine atoms. α-$AlF_3{\cdot}3H_2O$ has been shown to convert readily, at ambient temperatures, to the β- phase.[25] In the previous NMR study of aluminum fluoride trihydrate, the aluminum local environment was assumed to comprise octahedral $AlF_3(OH_2)_3$ groups, although the diffraction data for this compound were not presented.[15] The authors assumed that the metastable α-phase was present, bringing into question the assignments of the ^{19}F and ^{27}Al shift for this compound. This apparent discrepancy in the literature regarding the identification of aluminum fluoride trihydrate as a standard in NMR measurements has spurred us to reinvestigate the structure and obtain the NMR spectra for this compound.

Despite the confusion concerning the structures of the bulk $AlF_3{\cdot}3H_2O$ phases, a variety of highly crystalline fluorine-containing aluminum phosphates with isolated octahedral aluminum environments, $AlO_{6-x}F_x$ ($x = 1-3$), have been

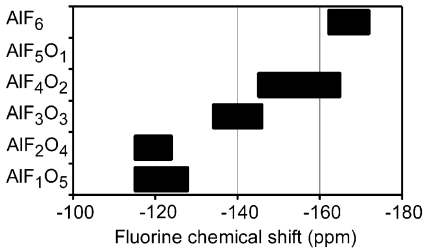

Figure 1. Typical ^{19}F chemical shifts of octahedral aluminum environments with oxygen and fluorine in the first coordination sphere, $AlO_{6-x}F_x$, versus x.

reported, with well-determined crystal structures. In general these materials contain fluorine in bridging Al−F−Al environments or terminal Al−F environments, where fluorine is coordinated via a single bond to aluminum. Taulelle and coworkers reported the structure of $AlPO_4$–CJ2, which contains isolated pairs of corner-connected $AlO_{6-x}F_x$ ($x = 1$ and 2) octahedra.[30] A ^{19}F chemical shift of −115 ppm was observed for bridging fluorine (Al−F−Al) in an AlO_5F_1 or AlO_4F_2 environment, while shifts of −121 and −124 ppm were observed for terminal fluorine in AlO_5F_1 and AlO_4F_2 environments, respectively. Dumas et al. reported a shift of −128 ppm for a bridging fluorine with an AlO_5F_1 environment.[31] Last, Simon et al. reported a shift of −140 ppm for the average environment AlO_3F_3.[32] These data have been compiled in Figure 1 and provide a partial chemical shift scale for ^{19}F.

Experimental Section

Preparation of Fluorinated Samples. Zinc-impregnated γ-Al_2O_3 starting materials were prepared as described in the following general procedure. A 100 g portion of 1/12 in. γ-Al_2O_3 extrudates was dried at 110 °C for approximately 16 h. The dried extrudate was added to a solution containing 4.16 g of $ZnCl_2$ in 85.70 g of water. The resulting mixture was dried at 110 °C overnight.

The γ-Al_2O_3 and the zinc-impregnated alumina (Zn/Al_2O_3) samples were fluorinated as follows. Approximately 9.0 g of γ-Al_2O_3 (or Zn/Al_2O_3) was loaded into a 0.5 in. i.d. inconel reactor, and the reactor was placed into a heated sand bath. The sand bath was gradually heated to 400 °C under a N_2 flow of 100 mL/min. The temperature was lowered to 100 °C, at which point flow of a HF/N_2 mixture was initiated at 100 mL/min. The temperature was gradually raised to 400 °C over an 8 h period and maintained at 400 °C for an additional 2 h. The procedure was performed using six different HF/N_2 (volume/volume) ratios for the Zn/Al_2O_3 samples, 50/50, 40/60, 30/70, 20/80, 10/90, and 5/95. From here on the fluorinated samples will be specified as starting material/% HF by volume. For example, Zn/20 indicates the Zn-impregnated Al_2O_3 sample fluorinated with 20% HF in nitrogen. Two different HF/N_2 ratios were used for the γ-Al_2O_3 samples, 50/50 and 10/90. The sample designated as Al_2O_3/10LT was prepared at lower temperature to achieve the same fluorine loading as Zn/10. The sample Al_2O_3/10LT was prepared by heating γ-Al_2O_3 under N_2 to 175 °C, at which point HF flow was initiated and continued for an additional 1 h after HF was detected in the reactor effluent. These conditions are identical to those used to prepare the samples whose catalytic activities are described in Table 1.

The sample surface area was determined by N_2 physisorption according to the BET method, by using a Micromeritics ASAP 2010 volumetric sorption analyzer. Chemical analyses for Al and Zn were obtained from ICP results, and the F content was determined by using an ion-selective electrode. The F content for the non-Zn-containing samples was determined from the ^{19}F NMR spectra by spin counting (i.e., the intensity of the spectra were compared with those of a known weight of α-AlF_3). The data are collected in Table 2.

TABLE 2: Sample Composition and Surface Properties

sample	F/Al ratio	wt % Zn	surface area (m^2/g)	concn of Lewis acid sites ($\mu mol/m^2$)
Al_2O_3/50	3.0	0	31.4	1.2
Al_2O_3/10	3.0	0	29.5	1.3
Al_2O_3/10LT	1.9	0	79.8	2.0
Zn/50	2.85	1.29	28.7	3.3
Zn/40	2.90	1.31	28.5	3.0
Zn/30	2.99	1.18	31.4	3.5
Zn/20	2.48	1.16	31.0	3.6
Zn/10	1.95	1.28	78.0	2.9
Zn/5	1.39	1.56	123.7	2.4

Phosphine Loading. Dimethylphenylphosphine (Aldrich) was used as the probe molecule for the study of the acidity of the fluorinated alumina samples. The fluorinated alumina samples were dried under vacuum to remove any residual surface water under the following conditions: 1 °C/min to 300 °C, hold at 300 °C for 4 h. Once dried, the samples were immediately moved into a dry atmosphere glovebox for further handling. Phosphine loadings were made directly onto the samples in the glovebox with a microliter syringe with 0.05 μL accuracy. Appropriate phosphine loading levels were estimated by taking into account the known surface area, to ensure that sufficient phosphine was loaded to bind to all acid sites, but that the signal due to the acid sites was not overwhelmed in the ^{31}P NMR spectra by the resonance from the physisorbed molecules. The samples were immediately sealed in 5 mm NMR rotors with airtight spacers. The samples were allowed to equilibrate for 1 h before the spectra were acquired.

X-ray Powder Diffraction. X-ray synchrotron powder diffraction data were collected at the X7B beamline at the National Synchrotron Light Source (NSLS), Brookhaven National Laboratory (BNL). A MAR-345 image plate (IP) detector mounted normal to the beam path was used to collect full-circle powder patterns. An external LaB_6 standard was used to determine the tilt angle, sample to detector distance, wavelength, and tilting angle of the IP. Integration of the full-circle powder patterns was performed with Fit-2d.[37] Rietveld refinement of the $AlF_3 \cdot 3H_2O$ phase was performed with GSAS.[38] The background was fit with a Chebyschev polynomial using 20 coefficients, and profile coefficients were fit with a pseudo-Voight function. Starting atomic coordinates were taken from those previously reported for the mineral rosenbergite.[27]

NMR. ^{27}Al and ^{19}F MAS NMR and $^{19}F/^{27}Al$ HETCOR NMR experiments were performed with a doubly tuned 2.5 mm Bruker probe on a Bruker Avance 600 (14.1 T) spectrometer. ^{27}Al and ^{19}F NMR spectra were collected at operating frequencies of 156 and 564 MHz, respectively. Zirconia rotors and spinning speeds of 35 kHz were used. Small ^{27}Al flip angles were used (<15°) to ensure uniform excitation of all spins. ^{27}Al and ^{19}F chemical shifts are referenced to 1.0 M aqueous aluminum sulfate and hexafluorobenzene as external standards at 0.0 and −163.0 ppm, respectively. Cross-polarization (CP) was used to transfer magnetization from ^{19}F to ^{27}Al for the $^{19}F/^{27}Al$ HETCOR NMR experiments. The Hartmann−Hahn condition for the $^{19}F/^{27}Al$ HETCOR experiments was determined with anhydrous aluminum fluoride and optimized for the so-called fast spinning regime.[39] The typical contact time was approximately 100 μs for MAS frequencies of 35 kHz. Repetition times of 1 s were used.

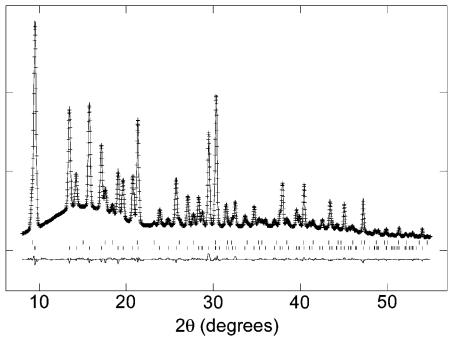

Figure 2. Refinement of β-$AlF_3 \cdot 3H_2O$ ($\lambda = 0.9033$ Å): observed (short horizontal lines), calculated (line), and difference (bottom line) diffraction profile, of the X-ray diffraction data. The positions of the reflections of β-$AlF_3 \cdot 3H_2O$ (bottom set) and the pyrochlore phase (top set) are shown under the pattern as vertical lines.

TABLE 3: Crystallographic Information for β-$AlF_3 \cdot 3H_2O$

cryst syst	tetragonal	wavelength, Å	0.902
space group	*P*4/*n*	2θ range, deg	8−55
Z	2	χ^2	2.334
cell params		R	0.0536
a, Å	7.71648(8)	R_p	0.0177
c, Å	3.64739(6)	R_{wp}	0.0230
density, g·cm^{-3}	2.111		

^{1}H-decoupled ^{31}P MAS NMR experiments were performed with a doubly tuned 5.0 mm Chemagnetics probe on a CMX-360 spectrometer at operating frequencies of 360.03 MHz for ^{1}H and 145.45 MHz for ^{31}P. Chemical shifts are referenced to tetramethylsilane (TMS) and 85% H_3PO_4 as external standards at 0.0 ppm. Zirconia rotors and spinning speeds of 10 kHz were used for all experiments. Samples were moved directly from a dry atmosphere glovebox to the NMR probe, where dry nitrogen was used for the purge and spinning gases. All spectra were acquired at −130 °C, using Chemagnetics variable-temperature equipment. The number of acid sites on the surface of the samples was quantified by deconvolution and integration of the ^{31}P resonances, taking into account the phosphine loading level, surface area, and mass of the sample.

Results

Structural Refinement of β-$AlF_3 \cdot 3H_2O$ and Determination of the ^{19}F Chemical Shift Scale. *XRD*. A diffraction pattern of a commercial sample of $AlF_3 \cdot 3H_2O$ was collected and compared to known patterns of the hydrates of aluminum trifluoride. Good agreement was observed between the experimental pattern and that reported for β-$AlF_3 \cdot 3H_2O$. No atomic coordinates have been reported for synthetic β-$AlF_3 \cdot 3H_2O$ though it is understood to be isostructural to β-$FeF_3 \cdot 3H_2O$.[26] In a survey of the literature, the mineral rosenbergite was found to have a cell and composition identical to those of β-$AlF_3 \cdot 3H_2O$; therefore, refinement was commenced using the atomic coordinates and unit cell of this mineral.[27] All the reflections could not be indexed on the basis of the tetragonal cell of this mineral, and a second cell corresponding to the cubic pyrochlore structure of the aluminum hydroxyfluoride AlF_2OH[28] was added to the refinement as a second phase, for which only the profile coefficients and phase fraction were refined. Satisfactory convergence of the refinement could not be obtained until hydrogen atoms were added to the hydrate structure. The final refinement is shown in Figure 2, and the details are given in Table 3. The final refinement produced a structure identical to that of rosenbergite with chains of corner-linked $AlF_4(OH_2)_2$ octahedra held together by hydrogen-bonded interstitial water molecules. Fluorine atoms are located in two positions, in the Al−F−Al bridges and in the disordered terminal equatorial positions. The four equatorial positions are disordered with two fluorine atoms and two water molecules (the atomic coordinates are given in the Supporting Information).

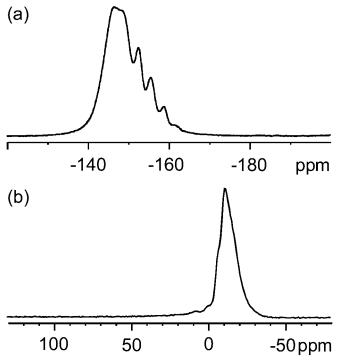

Figure 3. (a) ^{19}F MAS NMR and (b) ^{27}Al MAS NMR spectra of β-$AlF_3 \cdot 3H_2O$.

NMR. The ^{19}F and ^{27}Al MAS NMR spectra of β-$AlF_3 \cdot 3H_2O$ are shown in Figure 3. The ^{19}F MAS NMR spectrum (Figure 3a) is remarkably complex considering the fact that there are only two unique crystallographic fluorine sites. There appear to be at least six local environments with chemical shifts ranging from −145 to −160 ppm. We attribute the large chemical shift dispersion to different cis/trans ordering of fluorine in the equatorial positions with diverse hydrogen-bonding arrangements. The ^{27}Al MAS NMR spectrum of this phase (Figure 3b) shows a single resolved peak at approximately −13 ppm, with a line shape that indicates a distribution of QCCs (quadrupole coupling constants). Further studies are under way to decipher fluorine ordering and hydrogen-bonding arrangements in β-$AlF_3 \cdot 3H_2O$.

The ^{19}F chemical shift for this compound is compared with the data in the literature for crystalline compounds in Figure 1. A clear trend between the number of fluorine atoms coordinated to aluminum and the fluorine chemical shift, which moves up from approximately −120 ppm for AlO_5F to approximately −170 ppm for AlF_6, is observed.

X-ray Powder Diffraction of the Fluorinated Catalysts. The X-ray diffraction patterns of all the samples are shown in Figure 4. The Al_2O_3/50 sample (prepared in a feed stream of 50% HF in N_2) shows reflections predominately attributable to α-AlF_3; the additional reflections marked by the dashed lines are assigned to β-AlF_3. In contrast, the sample Al_2O_3/10LT shows no reflections from α-AlF_3. The major reflections observed in this sample are from the γ-Al_2O_3 starting material. A single reflection is present in this sample that has the same *d* spacing as a characteristic reflection from β-AlF_3, though the other reflections from β-AlF_3 are noticeably absent.

The fluorinated zinc-impregnated samples show some interesting trends. Zn/50 is similar to Al_2O_3/50 in that reflections from both α-AlF_3 and β-AlF_3 are present, with α-AlF_3 representing the majority phase. However, significantly more β-AlF_3 is present in the Zn/50 sample than in the Al_2O_3/50 sample. Moving from the Zn/50 sample to the Zn/40 and Zn/30 samples, a decrease in the amount of β-AlF_3 is seen, with α-AlF_3 still representing the majority phase in both samples. The samples Zn/20, Zn/10, and Zn/5 show remarkably different structural chemistry. In addition to α-AlF_3, a phase is observed which indexes as the cubic pyrochlore phase AlF_2OH (or η-AlF_3). The lattice parameters extracted for Zn/20, Zn/10, and

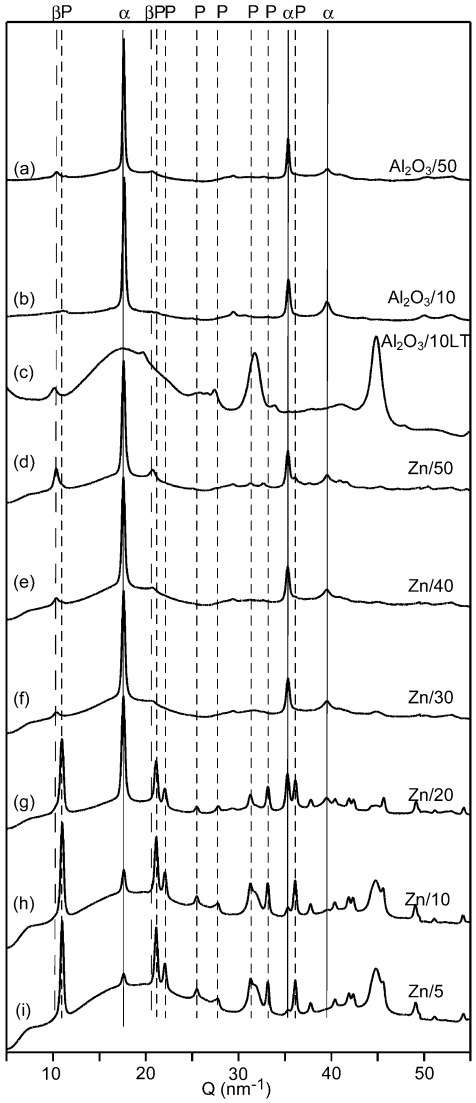

Figure 4. X-ray powder diffraction patterns of the fluorinated samples collected with $\lambda = 0.93$ Å. Intensity vs Q has been used for ready comparison of diffraction patterns collected at slightly different wavelengths. The solid vertical lines show the major reflections from α-AlF_3 (α), the large dashed lines show major reflections from β-AlF_3 (β), and the small dashed lines show reflections from the pyrochlore phase (P).

Zn/20 (9.80−9.82 Å) suggest that it is AlF_2OH (9.75−9.86 Å[28]) rather than η-AlF_3 (9.62 Å[19]); this is consistent with the NMR data, described later. The fraction of α-AlF_3 decreases to a minority contribution from Zn/20 to Zn/5.

^{19}F and ^{27}Al MAS NMR of the Fluorinated Samples. ^{19}F MAS NMR spectra are shown in Figure 5a−i, and ^{27}Al MAS NMR spectra are shown in Figure 5j−r. With respect to the fluorinated γ-Al_2O_3 samples, different fluorine and aluminum environments are observed depending on the conditions of fluorination and composition of the starting materials. The more fully fluorinated materials, for example, Al_2O_3/50 (Figure 5a,j) or Zn/50 (Figure 5d), show ^{19}F and ^{27}Al chemical shifts in the range observed for bulk aluminum fluorides, at −172 and −16 ppm, respectively. Nevertheless, even in the most fluorinated materials, minor resonances are present in the ^{19}F MAS NMR spectra with shifts from −145 to −165 ppm, consistent with aluminum hydroxyfluoride environments (see Figure 1). The zinc-impregnated samples fluorinated with lower concentrations of HF (e.g., Zn/20, Zn/10, and Zn/5) show increased concentrations of fluorine sites with chemical shifts between −145 and −165 ppm, again consistent with aluminum hydroxyfluoride environments. The ^{27}Al MAS NMR spectra of γ-Al_2O_3/10LT, Zn/10, and Zn/5 show peaks from both γ-Al_2O_3 sites, at approximately 8 (octahedral) and 60 ppm (tetrahedral), and additionally one from bulk aluminum fluoride at −16 ppm. Contributions from γ-Al_2O_3 are present in all the fluorinated samples, though at extremely low concentrations in those fluorinated with 50% HF. The ^{27}Al resonance attributable to bulk AlF_3 in the Al_2O_3/10LT sample is broader than that in Zn/10 and Zn/50. This resonance is assigned to amorphous AlF_3, on the basis of the XRD results, which showed no crystalline phases of AlF_3. Samples Zn/10 and Zn/5 also contain resolvable sites with chemical shifts between those of AlF_3 and γ-Al_2O_3. Again, this is indicative of aluminum hydroxyfluoride environments, $Al(OH)_xF_{6-x}$ ($1 < x < 6$), and is consistent with the formation of the AlF_2OH pyrochlore phase, as observed by XRD.

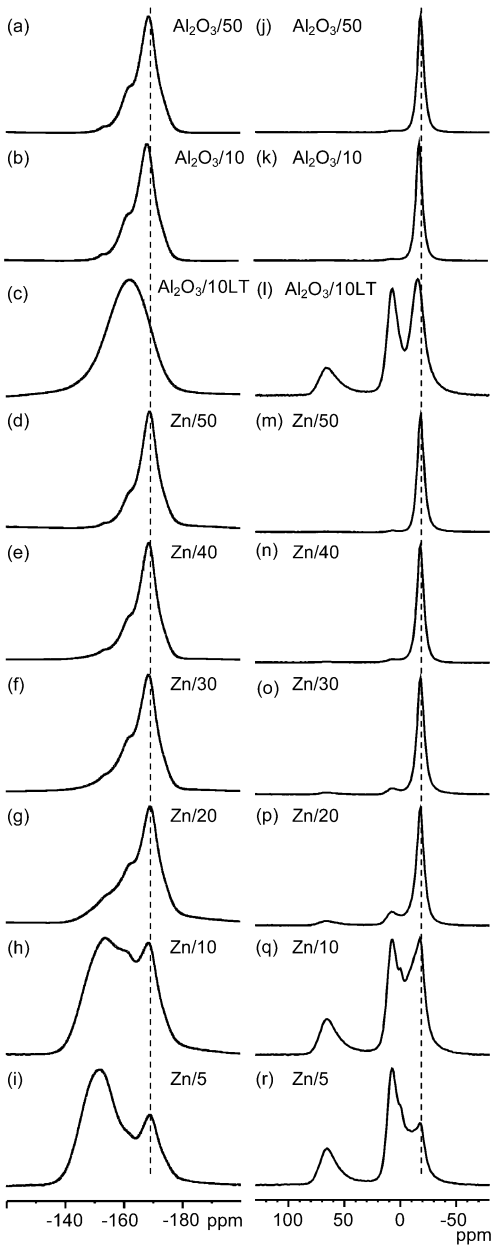

Figure 5. ^{19}F MAS NMR and ^{27}Al MAS NMR spectra of the fluorinated catalysts. The guidelines are shown at the ^{19}F and ^{27}Al chemical shift positions of bulk anhydrous aluminum fluoride at −172 and −16 ppm, respectively.

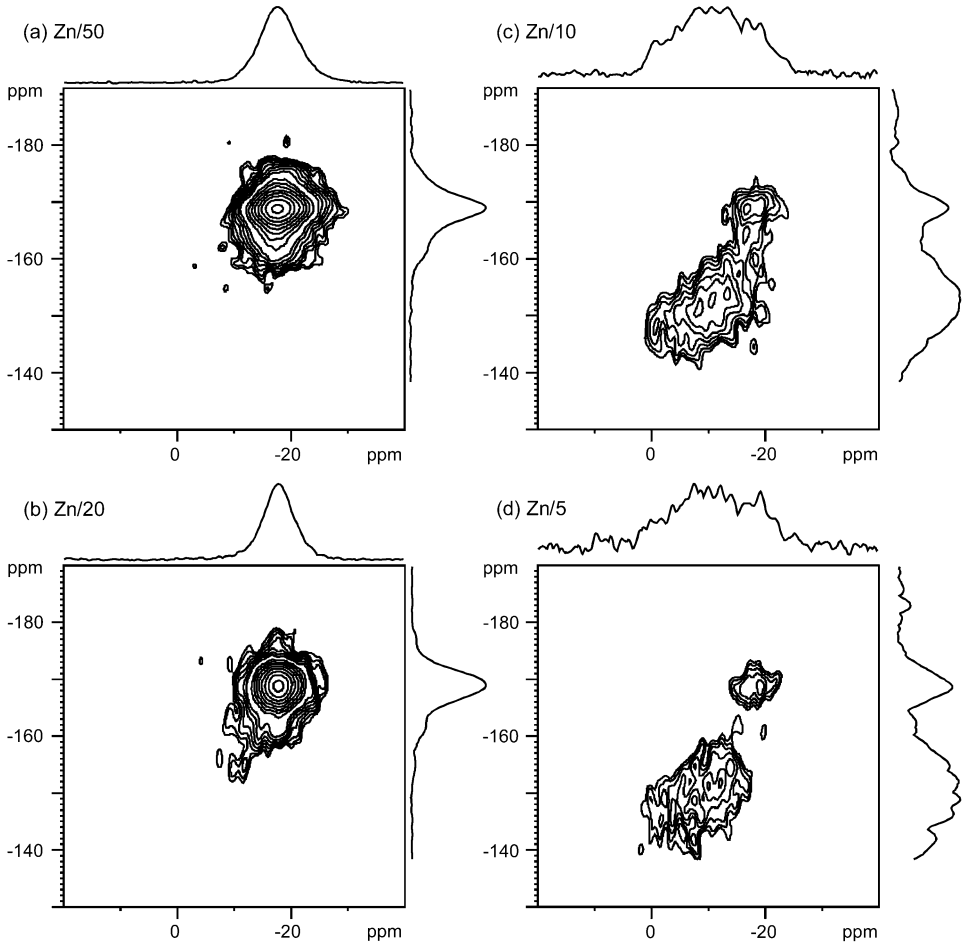

Figure 6. $^{19}F/^{27}Al$ HETCOR NMR two-dimensional spectra of Zn-impregnated samples.

$^{19}F/^{27}Al$ HETCOR NMR Spectroscopy. The $^{19}F/^{27}Al$ HETCOR spectra for the samples Zn/50, Zn/20, Zn/10, and Zn/5 are shown in Figure 6 and provide a method for identifying the Al atoms in close proximity to fluorine. A short contact time ensures that the major peaks in the spectrum correspond to directly bonded Al−F species. 2D $^{19}F/^{27}Al$ HETCOR NMR spectra were acquired for samples containing a large fraction of aluminum hydroxyfluoride environments. Sample Zn/50 represents the one exemplar sample where the HETCOR spectrum was collected for a highly fluorinated sample. Since there is only one predominant fluorine and aluminum site, the spectrum does not provide any additional information over that obtained from the simple one-pulse experiments described above.

The spectra of the Zn/10 and Zn/5 samples illustrate the utility of this type of correlation experiment for samples with different fluorine and aluminum environments. The fluorines with chemical shifts between −140 and −160 ppm are correlated to the aluminum sites with chemical shifts between 0 and −15 ppm. The ^{19}F chemical shifts become more negative as the aluminum chemical shifts move toward more negative values. For example, fluorine chemical shifts of −150 and −160 ppm correlate with aluminum chemical shifts of −5 and −15 ppm, respectively. The chemical shifts then move toward those of bulk AlF_3, −172 (^{19}F) and −16 (^{27}Al) ppm. This is consistent with the compiled ^{19}F chemical shift ranges shown in Figure 1. There was no cross-peak between the ^{19}F signals and the ^{27}Al resonances due to the residual γ-Al_2O_3 in these samples, indicating that the γ-Al_2O_3 is not near fluorine and represents an, at least locally, segregated phase.

^{31}P MAS NMR. Proton-decoupled ^{31}P MAS NMR spectra (Figure 7) were collected at −130 °C for all samples, to freeze out motion of the phosphine molecules on the surface and prevent exchange between multiple sites. Different sites are clearly visible, including one at approximately −45 ppm that results from physisorbed/free phosphine not bound to a Brønsted or Lewis acid site. Phosphine molecules bound directly to Lewis acid sites give rise to the resonance at approximately −35 ppm. In some samples a very weak resonance is observed at 0 ppm, which is a result of the protonated phosphine ion bound directly to the conjugate base of the Brønsted acid (surface) site. The concentration of acid sites obtained by integration of the −35 ppm resonance and the measured surface areas are listed in Table 2.

Discussion

It is clear from the XRD results that the structural phase of the fluorinated material is highly dependent on the starting material, the series of fluorinated Zn-impregnated samples clearly illustrating that the fluorination conditions can also affect the structure of the final fluorinated material. Three distinct phases have been identified in the fluorinated Zn-impregnated samples, α-AlF_3, β-AlF_3, and the pyrochlore phase. These phases vary in relative concentration depending on the fluorination conditions. The Zn/50 sample clearly contains more β-AlF_3 than does the Al_2O_3/50 sample. This observation is consistent with reports in the patent literature, where the overall concentration of β-AlF_3 was shown to increase as the quantity of Zn in

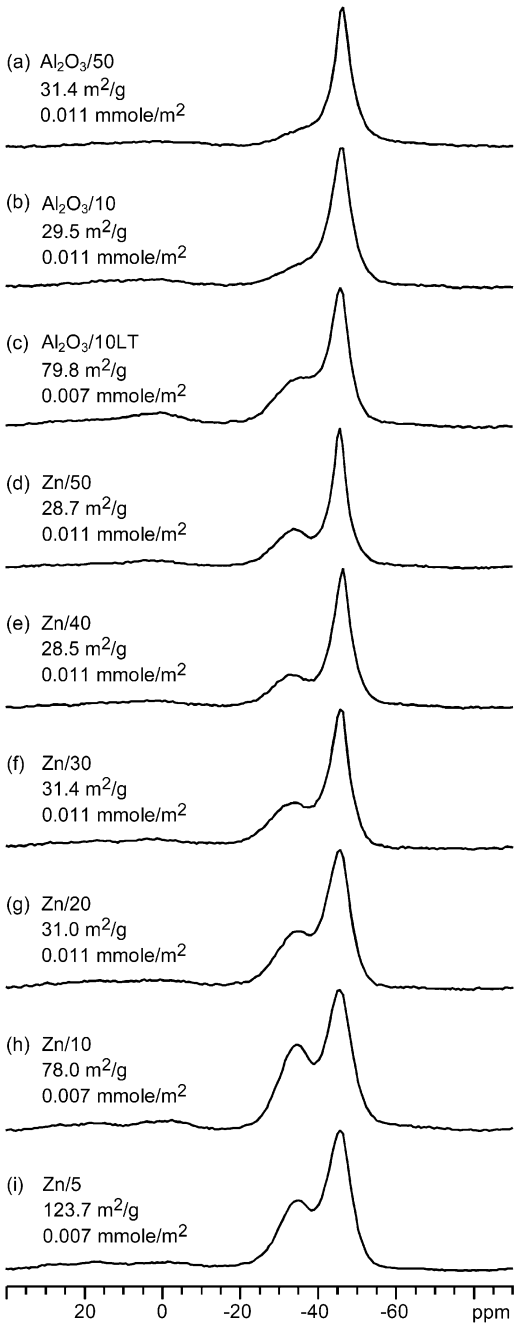

Figure 7. ^{1}H-decoupled ^{31}P NMR spectra, (BET) surface area and Lewis acid site concentration (from NMR).

the starting material increases, when the materials were fluorinated with less than 50% HF (Table 1).[2−5] Thus, the presence of Zn in the starting material appears to be important in directing the formation of the β-AlF_3 phase (for fluorination conditions of 50% HF). When HF concentrations under 30% are used, the pyrochlore phase, and not the β-AlF_3 phase, is observed in the final product in this study, when the starting material contains zinc. In general, higher concentrations of HF tend to favor the bulk aluminum fluoride phases.

The ^{19}F spectrum of the model compound β-$AlF_3{\cdot}3H_2O$ illustrates that many different factors contribute to the fluorine chemical shifts in aluminum hydroxyfluorides, including fluorination level, H−F hydrogen bonding, and local geometry. Nonetheless, the compiled ^{19}F chemical shifts for octahedral aluminum environments containing both fluorine and oxygen in the Al first coordination shell (Figure 1) show a general trend, moving from −120 ppm for the environment with the lowest number of fluorine atoms (an octahedral AlO_5F_1 environment) toward bulk aluminum fluoride (an octahedral AlF_6 environment) at −172 ppm.

All the fluorinated samples contain ^{27}Al and ^{19}F resonances in the range that is attributable to octahedral AlF_6 environments (−17 and −171 ppm, respectively). Fluorine environments with ^{19}F shifts from −140 to −160 ppm are observed even for the highly fluorinated samples such as Al_2O_3/50 or Zn/50, which is indicative of residual framework oxygen. This is supported by the F/Al ratios determined from elemental analyses (Table 2) and the ^{27}Al NMR spectra of these samples where weak resonances at approximately 0 ppm are observed. Under milder HF fluorination conditions (i.e., when the HF concentration in the feed stream is decreased), more oxygen remains either as a structural impurity (e.g., in the pyrochlore phase) or in a segregated phase (e.g., as residual γ-Al_2O_3 in Al_2O_3/10LT).

The Zn-impregnated samples Zn/20, Zn/10 and Zn/5 have all been shown by XRD to contain significant quantities of the pyrochlore phase. The ^{19}F MAS NMR spectra of these samples are dominated by resonances with chemical shifts between −140 and −160 ppm from aluminum sites in mixed fluorine/oxygen environments. This assignment is supported by the ^{27}Al MAS NMR and ^{19}F/^{27}Al HETCOR NMR spectra. On the basis of Figure 1, the most intense resonance in the ^{19}F NMR spectra of Zn/5 and Zn/10 at −150 ppm is assigned to the site AlF_4O_2, consistent with the environment in the pyrochlore structure. Examining the HETCOR spectra in more detail, two groups of resonances are assigned, one centered around that of bulk AlF_6 and one due to $AlF_{6-x}O_x$ groups. The low-frequency shoulder on the AlF_6 resonance (at −162 ppm) (clearly visible in the HETCOR spectra of Zn/50 and Zn/20) is associated with an ^{27}Al resonance with a shift (−19 ppm) that is similar to that in bulk AlF_6, suggesting that this environment may be due to disorder (caused by residual O^{2-}/OH^- groups) in the AlF_6 phase. The second group of resonances (with ^{27}Al resonances of 0 to −15 ppm) is assigned to the pyrochlore phase.

A comparison of the ^{19}F and ^{27}Al MAS NMR spectra of the Al_2O_3/10LT and Zn/10 samples, which contain similar fluorine contents, reveals noticeable differences. First, the ^{27}Al MAS NMR spectrum of Al_2O_3/10LT contains signals from γ-Al_2O_3 and from what appear, on the basis of ^{27}Al NMR, to be AlF_6 groups. In contrast, the ^{27}Al MAS NMR spectrum of Zn/10 contains resonances from sites with chemical shifts intermediate between those of AlO_6 and AlF_6 groups. The ^{19}F MAS NMR spectrum of Al_2O_3/10LT is much broader than the resonance of crystalline AlF_3 and shifted away from a typical shift position to −163 ppm. Although this shift suggests the presence of aluminum oxy/hydroxyfluoride environments, this is not consistent with the Al NMR spectrum. The ^{19}F spectrum of a highly disordered sample of AlF_3 obtained by plasma synthesis shows a broad resonance at −171 ppm with a broad shoulder at lower frequencies, suggesting that the −163 ppm resonance of Al_2O_3/LT may be assigned to amorphous AlF_3.[40] The XRD pattern of Al_2O_3/10LT is dominated by the γ-Al_2O_3 reflections, again suggesting that the fluorinated phase is amorphous.

In our recent report, we showed by using in situ X-ray diffraction that the fluorination of γ-Al_2O_3 with HCFC-22 yields a disordered α-AlF_3 material, and not the β-AlF_3 or pyrochlore phases.[10] The formation of bulk AlF_3 under these conditions

becomes clear if the following reactions are considered:

$$Al_2O_3 + 3HCF_2Cl \rightarrow 2AlF_3 + 3HCl + 3CO \quad (1)$$

$$Al_2O_3 + 4HF \rightarrow 2AlF_2OH + H_2O \quad (2)$$

$$Al_2O_3 + 6HF \rightarrow 2AlF_3 + 3H_2O \quad (3)$$

When HCFC-22 is used as a fluorinating agent, the hydrogen and chlorine atoms on the fluorinating molecule are removed through the elimination of the volatile product HCl (eq 1). When low concentrations of HF are used as the fluorinating agent, the pyrochlore is clearly a reasonable intermediate (see eq 2), but it is difficult to write a plausible reaction to justify its formation in significant quantities when HCFC-22 is used. The formation of the pyrochlore phase appears to be correlated with the presence of acidic protons. This suggestion is supported by the work of Saniger et al., who reported that the fluorination of alumina under low pressures of F_2 at ambient temperatures also leads to the formation of the pyrochlore phase.[6] In this system, any protons present on the surface of the alumina will be unlikely to be removed as water under low pressures of gaseous F_2 and ambient temperature, favoring the formation of hydroxyfluorides.

Surprisingly, the presence of protons on the surface (or in the bulk) of the starting material, or the use of an acidic fluorinating agent, also appears to favor the formation of the metastable phase β-AlF_3 (over α-AlF_3) even when the final product contains no or few hydroxyl groups. This is supported by many examples in the literature. β-AlF_3 can be prepared from the ammonium salt of AlF_3 or from the proton-containing material $AlF_3 \cdot 3H_2O$ at low temperatures.[20] Additionally, ammonium fluoride impregnation has also been used to prepare fluorinated aluminas. Decanio et al. have shown that ammonium salts of aluminum fluoride (i.e., $(NH_4)_3AlF_6$) form on the surface and when calcined yield β-AlF_3.[6] This result is consistent with the method used to prepare metastable phases of AlF_3, which may be synthesized by decomposition of ammonium salts of AlF_3.[22,23] Again, depending on the calcination conditions,[22] NH_3 will first be removed, leaving acidic protons, the intermediate reacting further to form β-AlF_3.

The formation of particular structures can be rationalized by considering the differences in local structure of the fluorinated phases. The thermodynamically stable α-AlF_3 phase, which adopts the rhombohedrally distorted ReO_3 structure, is characterized by four-membered rings comprising Al−F−Al bridges (i.e., $(Al-F-)_n$, $n = 4$). The β-AlF_3 phase contains three- and six-membered ring systems which occur in planes that stack along the *c*-axis, as shown in Figure 8a. The planes of three- and six-membered rings are linked via four-membered ring systems that form parallel to the stacking direction, resulting in a one-dimensional six-membered ring channel system along the *c*-axis. The pyrochlore structure, which contains three- and six-membered rings only, is shown in Figure 8c and consists of interconnecting channel systems formed from six-membered rings. Structures with three-membered rings have characteristic Al−F−Al bond angles (141°) which are smaller than those observed in the four-membered rings found in the room-temperature structure of α-AlF_3 (158°). These rings are more strained than in the thermodynamically stable α-AlF_3 phase. Protonated Al−O(H)−Al groups typically show smaller bond angles than Al−F−Al groups, which appears to favor the formation of final products with Al−X−Al (X = F or OH) linkages with smaller bond angles, as found in the pyrochlore and β-AlF_3 phases, as opposed to the α-AlF_3 phase. If significant concentrations of hydroxyl groups are already present (as found in high surface area aerogels), then some β-AlF_3 is formed even when a nonacidic fluorinating agent such as HFC-23 is used, which is consistent with our proposal.[7]

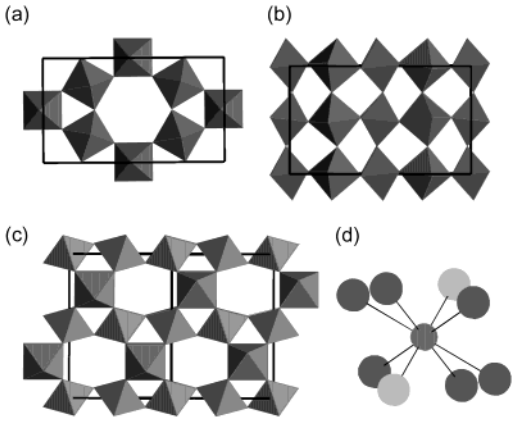

Figure 8. β-AlF_3 and the pyrochlore phase AlF_2OH: view down (a) the [001] direction of β-AlF_3, (b) the [100] direction of β-AlF_3 and (c) the [110] direction of the cubic pyrochlore phase. (d) A site of the pyrochlore structure showing the coordination of the A cation (center) to six X (F^- of OH^-) sites (dark spheres) and two X′ sites (light spheres). Both the A and X′ sites are vacant in AlF_2OH and η-AlF_3.

The question that still remains to be addressed is how the Zn^{2+} acts to favor the increased formation of the pyrochlore structure at low HF concentrations and β-AlF_3 at higher concentrations. Zn^{2+} is incorporated by impregnation with $ZnCl_2$, the chloride ions being removed in the form of HCl, when the material is calcined. Since $ZnCl_2$ is acidic it may, when impregnated on the surface, be important in stabilizing or increasing the concentration of bridging (acidic) hydroxyl groups (i.e., Al−O(H)−Al), favoring the formation of the three-membered rings found in the β-AlF_3 and pyrochlore phases. The locations of the Zn cations in the fluoride structures were not determined in this study. In AlF_2OH, the A and X′ sites of the $A_2B_2X_6X'$ pyrochlore structure are vacant, the Al and F/OH groups occupying the B and O sites, respectively (Figure 8c). The H atoms of the OH groups will be located in the puckered six-membered rings, the vacant A (16d) site lying in the center of the ring. The F−F(OH) interatomic distance across the ring is 4.8 Å, indicating that the A site is slightly too large for the Zn^{2+} cation. However, given the number of vacancies already present in this structure, it seems unlikely that all of the Zn^{2+} cations would replace Al^{3+} in the B site, creating further anion vacancies. Therefore A cation substitution represents a possible doping site for Zn^{2+} (Figure 8d). The ideal A site is eight-coordinate, if both the X′ (8d) sites are also occupied. In the case of Zn^{2+} doping on this site, the X′ sites could be filled by the hydroxyls or fluoride ions required to charge balance the Zn^{2+} ion (Figure 8d). Given the small size of Zn^{2+}, either the ions located in the 8d (O′) sites will be displaced off their normal sites to form two shorter Zn−O′ bonds or the Zn^{2+} may be displaced slightly off the ideal site into the tetrahedral site formed by two framework anions and two anions on the 8d site. The six-membered rings in the β-AlF_3 structures are slightly larger (the F−F distances across the rings are 5.05−5.11 Å), since the $(Al-F)_6$ rings are flat (Figure 8a). Thus, Zn^{2+} doping in this structure should be less energetically favorable. We suggest that the difference in the sizes of the vacant sites in these two structures may stabilize the pyrochlore phase over β-AlF_3 in the presence of Zn^{2+} cations. The α-AlF_3 structure contains a vacant eight-coordinate site in the center of the cube formed by the corner-connected AlF_6 octahedra. This is the A

site of the perovskite structure. This site is even less favorable for Zn substitution, since eight long Zn−F distances of 2.45−2.5 Å are formed, presuming that the Al−F−Al angles are unaffected by Zn^{2+} doping. In addition, it is not clear where the additional anion dopants (required for charge balance) would be accommodated in this structure. Thus, Zn^{2+} doping is unlikely to provide a driving force for α-AlF_3 formation. A second doping mechanism, which could be important for all the structures and which does not result in the creation of further anion vacancies, involves the substitution of the neutral species $Zn[(F/OH)_2(OH_2)]$ onto the $Al[F_3]$ sites. This should result in the formation of $Zn-O(H_2)$---Al^{3+} linkages with very weak O---Al^{3+} bonds. This mechanism represents one plausible method for generating Lewis acid sites in the presence of Zn^{2+}, particularly following the loss of the water molecules on calcination. Again, this mechanism should favor the formation of structures with three-membered rings and not α-AlF_3. EXAFS experiments are currently in progress to probe the local environment of Zn in these structures and test these hypotheses.

Some insight into the effects of cation impregnation and bulk phases on acidity can be ascertained from the ^{31}P MAS NMR results for the phosphine loaded-samples. The fluorinated Zn-impregnated samples clearly contain higher concentrations of Lewis acid sites than do the materials without zinc. This is best illustrated by the ^{31}P MAS NMR of dimethylphenylphosphine adsorbed on the samples Zn/50 and Al_2O_3/50. The Zn/50 sample contains nearly 3 times more acid sites than the material that lacks Zn. It is not, however, directly evident from a comparison of Zn/50 and Al_2O_3/50 whether the Zn is directly responsible for the formation of Lewis acid sites or whether they are due to the increased proportion of the β-AlF_3 phase in the Zn-containing material. Comparing Zn/30 with Al_2O_3/50, two materials with similar proportions of β-AlF_3 and α-AlF_3, significant differences in Lewis acidities are observed. The Zn/30 sample contains approximately 3 times the number of Lewis acid sites than does Al_2O_3/50. Moving down the series from Zn/50 to Zn/40 to Zn/30, the relative concentration of β-AlF_3 in the fluorinated samples decreases, although the concentration of Lewis acid sites remains approximately constant. Another useful comparison, even though the fluorinated phases present are different, is between Al_2O_3/10LT and Zn/20, which have similar fluorine contents and surface areas. Zn/20 has significantly more Lewis acid sites than does Al_2O_3/10LT. From the comparisons described above, we argue that it is not necessarily the structural phase that is important in fluorinated alumina catalysts; rather it is the local structural disorder that results in the formation of Lewis acid sites. The metastable phases that form as a result of Zn impregnation are not necessarily directly responsible for the formation of Lewis acid sites. It is more likely that the local structural disorder caused by the incorporation of the Zn leads to an increased concentration of coordinative unsaturated aluminum atoms.

Lewis acidity is thought to be important in the F/Cl exchange and addition reactions.[12,13] Kemnitz et al. have proposed that the OH groups of water, which are sometimes associated with Brønsted acidity, do not contribute to catalysis, but instead result in the destruction of the HCFC or CFC molecules and further fluorination of the surface. This is consistent with our ^{31}P MAS NMR results for the Zn samples, which show both enhanced catalytic activity *and* Lewis acidity, in comparison to the materials without Zn. Essentially no Brønsted acidity is observed. Our work is, however, in contradiction with work in the patent literature, which correlated activity with an increased β-AlF_3 concentration.[2−4]

In the work of Kemnitz and co-workers, surfaces with structures related to β-AlF_3 are proposed to be responsible for catalysis.[12,13] These surfaces may be present initially in β-AlF_3 or may grow during the low-temperature activation of the starting material (e.g., the pyrochlore phase or γ-Al_2O_3). β-AlF_3 formation in the Zn^{2+}-impregnated phases was also correlated with the catalytic activity in the patent literature.[2−4] The Lewis sites in the fluorinated phases are postulated to occur on the more readily accessible low-coordinate aluminum sites on β-AlF_3 (001) surfaces, in comparison to the (001) α-AlF_3 surfaces, where the Lewis acid sites are thought to be blocked by fluoride ions.[12,13] However, a new AlF_3 phase synthesized by Herron et al., κ-AlF_3, which contains only three-, four-, and five-membered rings also shows extremely high activity for Cl/F exchange reactions, indicating that the six-membered rings found in β-AlF_3 are not essential for catalytic activity. The observed increased Lewis acidity on β-AlF_3 or the other metastable phases is, in all likelihood, not directly related to the three-dimensional ordered structure as discussed above. We suggest that the conditions used to synthesize the metastable AlF_3 phases may also play an important role in controlling the creation and concentration of Lewis acid sites. For example, β-AlF_3 is synthesized from $AlF_3 \cdot 3H_2O$ at low temperatures, the β-AlF_3 framework forming as water is removed from the structure. Coordinatively unsaturated aluminum atoms may readily form during this dehydration process, and residual hydroxyls may remain, as suggested by IR evidence.[41]

Structural disorder and heterogeneity of the catalytically active fluorinated materials is a common theme in the literature. The κ-AlF_3 phase has been reported to be the most active phase for Lewis acid catalyzed F/Cl exchange reactions. While the refined structure clearly represents an accurate model, there are noticeable indications of local structural disorder in this material, which could include stacking faults or impurity phases. Whatever the origin of the local structural disorder, it becomes hard to argue whether it is the three-dimensional structure or inherent disorder that promotes the formation of catalytically active Lewis acid centers. While defect-free α-AlF_3, synthesized at high temperature, is known to show very poor catalytic activity, α-AlF_3 containing defects has been shown to be active for CFC-re-forming reactions.[10] Consequently, it seems that the occurrence of catalytic activity should be correlated to the number (and strength) of the Lewis acid sites rather than simply to the long-range crystallographic structure.

Conclusion

General trends for the ^{19}F chemical shifts of hydroxy/oxyfluorides of aluminum were established in this work, which should be of general use in this field. In particular, the fluorine local environments in β-$AlF_3 \cdot 3H_2O$ were established by structural refinement with synchrotron XRD data, allowing the ^{19}F chemical shifts for $AlF_4(OH_2)_2$ groups to be determined. The ^{19}F assignments were then used to identify various aluminum hydroxy/oxyfluoride environments in the fluorinated aluminas. $^{19}F/^{27}Al$ HETCOR NMR experiments were used to determine $^{19}F/^{27}Al$ connectivities, confirming the assignments and separating the groups of resonances from the pyrochlore and bulk AlF_3 phases.

Basic probe molecules (i.e., phosphines) were used to study acid sites on the surfaces of fluorinated alumina. Clear differentiation between Lewis and Bronsted acid sites was possible with this method, as well as quantification of the number of acid sites. Enhanced Lewis acidity was shown on the zinc-containing fluorinated aluminas, which correlated with the higher

catalytic activity of these materials for F/Cl exchange or addition reactions. Zn impregnation also resulted in an increase in the concentration of the pyrochlore phase following fluorination in dilute HF feeds and the β-AlF_3 phase in higher HF concentrations. We suggest that it is not necessarily the formation of these phases that results in the improved catalytic activity of these materials; instead we propose that it is the increased disorder in the structures resulting from the Zn^{2+} doping that gives rise to the higher Lewis acidity of these materials and their higher catalytic activity. More experiments are in progress to explore this hypothesis in a wider range of systems.

The work reported in this paper demonstrates that the structural chemistry of fluorinated aluminas is dependent on the starting material, the presence of transition-metal cations, and the nature of the fluorinating agent. The metastable pyrochlore and β-AlF_3 phases appear to be formed in greater concentrations from starting materials with increased numbers of acidic protons or with acidic fluorinating agents such as HF. Both cases lead to higher concentrations of Al−O(H)−Al linkages, which we propose favor the formation of hydroxyfluoride structures with three-membered rings, as found in the pyrochlore and β-AlF_3 phases, but not in the thermodynamic phase α-AlF_3. This hypothesis is supported by the synthetic routes used to synthesize these phases. The enhanced stability of the pyrochlore phase for the Zn^{2+}-impregnated samples fluorinated in low HF concentrations is ascribed to the presence of the vacant A site in this structure, which is slightly smaller than a similar vacant site in the β-AlF_3 structure. Substitution of species such as $ZnF_2(OH_2)$ for AlF_3 in these structures may represent one mechanism for creating Lewis acid sites.

Further studies are under way to understand the mechanisms of the formation of Lewis acidity in transition-metal-modified fluorinated aluminas in more detail and to explore the generality of the above proposals. In particular, the structure-directing abilities of different dopant ions in this and a wider range of chemistries, and the effect that this plays in catalysis, remain to be explored in greater detail.

Acknowledgment. Martine Ziliox is thanked for her assistance in the collection of the high-field NMR data. Financial support from the Basic Energy Sciences program of the Department of Energy (DOE) is gratefully acknowledged (Contract DEFG0296ER14681). The research at BNL was supported under Contract DE-AC02-98CH10886 with the DOE by its Division of Chemical Sciences, Office of Basic Energy Research. D.R.C. and V.N.M.R. acknowledge the technical assistance of J. Green, F. Walzcak, P. Ireland, J. Fleetwood, T. Borecki, P. Hollins, B. Hambleton, and K. Holzapfel.

Supporting Information Available: A table listing the atomic positions for β-$AlF_3 \cdot 3H_2O$ and a figure showing the β-$AlF_3 \cdot 3H_2O$ structure. This material is available free of the charge via the Internet at http://pubs.acs.org.

References and Notes

(1) Manzer, L. E. *Science* **1990**, *249*, 31−35. Manzer, L. E.; Rao, V. N. M. Catalytic Synthesis of CFC Alternatives. *Adv. Catal.* **1993**, *39*, 329. Kemnitz, E.; Menz, D. H. *Prog. Solid State Chem.* **1998**, *26*, 97−153.

(2) Corbin, D. R.; Rao, V. N. M. U.S. Patent 5,300,710, 1994.

(3) Corbin, D. R.; Rao, V. N. M. U.S. Patent 5,300,711, 1994.

(4) Corbin, D. R.; Rao, V. N. M. U.S. Patent 5,331,170, 1994.

(5) Corbin, D. R.; Rao, V. N. M. U.S. Patent 6,040,486, 2000.

(6) Saniger, J. M.; Sanchez, N. A.; Flores, J. O. *J. Fluorine Chem.* **1998**, *88*, 117.

(7) Skapin, T. *J. Mater. Chem.* **1995**, *5*, 1215−1222. Skapin, T.; Kemnitz, E. *Catal. Lett.* **1996**, *40*, 241−247.

(8) McVicker, G. B.; Kim, C. J.; Eggert, J. J. *J. Catal.* **1983**, *80*, 315−327.

(9) DeCanio, E. C.; Bruno, J. W.; Nero, V. P.; Edwards, J. C. *J. Catal.* **1993**, *140*, 84−102.

(10) Chupas, P. J.; Ciraolo, M. F.; Hanson, J. C.; Grey, C. P. *J. Am. Chem. Soc.* **2001**, *123*, 1694−1702.

(11) Deshmukh, S. S.; Kovalchuk, V. I.; Borovkov, V. Y.; d'Itri, J. L. *J. Phys. Chem. B* **2000**, *104*, 1277−1284.

(12) Hess, A.; Kemnitz, E.; Lippitz, A.; Unge, W. E. S.; Menz, D. H. *J. Catal.* **1994**, *148*, 270−280.

(13) Hess, A.; Kemnitz, E. *J. Catal.* **1994**, *149*, 449−457.

(14) Hedge, R. I.; Barteau, M. A. *J. Catal.* **1989**, *120*, 387.

(15) Fischer, L.; Harle, V.; Kastelan, S.; d'Espinose de la Caillerie, J. B. *Solid State NMR* **2000**, *16*, 85−91.

(16) Rodriguez, L. M.; Alcaraz, J.; Hernandez, M.; Ben Taarit, Y.; Vrinat, M. *Appl. Catal., A* **1998**, *169*, 15. Rodriguez, L. M.; Alcaraz, J.; Hernandez, M.; Dufaux, M.; Ben Taarit, Y.; Vrinat, M. *Appl. Catal., A* **1998**, *189*, 53−61.

(17) Corma, A.; Fornes, V.; Ortega, E. *J. Catal.* **1985**, *92*, 284−290.

(18) Matulewicz, E. R. A.; Kerkoff, F. P. J. M.; Moulin, J. A.; Reitsma, H. J. *J. Colloid Interface Sci.* **1980**, *77*, 110−119.

(19) Daniel, P.; Bulou, A.; Rousseau, M.; Nouet, J.; Fourquet, J. L.; Leblanc, M.; Burriel, R. *J. Phys.: Condens. Matter* **1990**, *2*, 5663−5677. Daniel, P.; Bulou, A.; Rousseau, M.; Nouet, J.; Fourquet, J. L.; Leblanc, M.; Burriel, R. *J. Phys.: Condens. Matter* **1990**, *2*, 5663−5677.

(20) Le Bail, A.; Jocoboni, C.; Beblanc, M.; De Pape, R.; Duroy, H.; Fourquet, J. L. *J. Solid State Chem.* **1988**, *77*, 96−101. Christoph, F. J.; Teufer, G. U.S. Patent 3,178,483, 1965.

(21) Shinn, D. B.; Crocket, D. S.; Haendler, H. M. *Inorg. Chem.* **1966**, *11*, 1927−1933.

(22) Herron, N.; Thorn, D. L.; Harlow, R. L.; Jones, G. A.; Parise, J. B.; Fernandez-Baca, J. A.; Vogt, T. *Chem. Mater.* **1995**, *7*, 75−83.

(23) Le Bail, A.; Fourquet, J. L.; Bentrup, U. *J. Solid State Chem.* **1992**, *100*, 151−159.

(24) Mootz, D.; Oellers, E. J.; Wiebcke, M. *Acta Crystallogr.* **1988**, *C44*, 1334−1337. Chandross, R. *Acta Crystallogr.* **1964**, *17*, 1477−1478.

(25) Ehret, W. F.; Frere, F. J. *J. Am. Chem. Soc.* **1945**, *67*, 64−68.

(26) Freeman, R. D. *J. Phys. Chem.* **1956**, *60*, 1152. Freeman, R. D. *J. Phys. Chem.* **1957**, *61*, 256.

(27) Rosenberg, P. E. *Am. Mineral.* **1988**, *73*, 855−860. Olim, F.; Sabelli, C.; Trosti-Ferroni, R. *Eur. J. Mineral.* **1993**, *5*, 1167−1174.

(28) Fourquet, J. L.; Riviere, M.; Le Bail, A.; Nygrens, M.; Grins, J. *Eur. J. Solid State Inorg. Chem.* **1988**, *25*, 535−540. Menz, D. H.; Mensing, Ch.; Hönle, W.; von Schnering, H. G. *Z. Anorg. Allg. Chem.* **1992**, *611*, 107−113.

(29) Karraker, D. G.; Smith, P. K. *Inorg. Chem.* **1992**, *31*, 1118−1120. Teufer, G. *Acta Crystallogr.* **1964**, *17*, 1480.

(30) Taulelle, F.; Pruski, M.; Amoureux, J. P.; Lang, D.; Bailly, A.; Huguenard, C.; Haouas, M.; Gerardin, C.; Loiseau, T.; Ferey, G. *J. Am. Chem. Soc.* **1999**, *121*, 12148−12153.

(31) Dumas, E.; Taulelle, F.; Ferey, G. *Solid State Sci.* **2001**, *3*, 613−621.

(32) Simon, N.; Guillou, N.; Loiseau, T.; Taulelle, F.; Ferey, G. *J. Solid State Chem.* **1999**, *147*, 92−98.

(33) Lunsford, J. H.; Rothwell, W. P.; Shen, W. *J. Am. Chem. Soc.* **1985**, *107*, 1540−1547.

(34) Yong, H.; Coster, D.; Chen, F. R.; Davis, J. G.; Fripiat, J. J. In *New Frontiers in Catalysis*; Guczi, G., Ed.; 1992; pp 1159−1170.

(35) Rahman, M. M.; Liu, H. Y.; Prock, A.; Giering, W. P. *Organometallics* **1987**, *6*, 650−658.

(36) Haw, J. F.; Zhang, J.; Shimizu, K.; Venkatraman, T. N.; Luigi, D.-P.; Barich, D. H.; Nicholas, J. B. *J. Am. Chem. Soc.* **2000**, *122*, 12561−12570.

(37) Hammersley, A. P. *FIT2D V9.129 Reference Manual V3.1*; ESRF Internal Report ESRF98HA01T; 1998. Hammersley, A. P.; Svenson, S. O.; Hanfland, M.; Hauserman, D. *High-Pressure Res.* **1996**, *14*, 235−248.

(38) Larson, A. C.; Von Dreele, R. B. *GSAS General Structure Analysis System*; Report LAUR 86-748; Los Alamos National Laboratory: Los, Alamos, NM, 1995.

(39) Vega, A. J. *Solid State Nucl. Magn. Reson.* **1992**, *1*, 17−32.

(40) Delattre, J. L.; Chupas, P. J.; Grey, C. P.; Stacy, A. M. *J. Am. Chem. Soc.* **2001**, *123*, 5364−5365.

(41) Demourgues, A.; Francke, L.; Durand, E.; Tressaud, A. *J. Fluorine Chem.* **2002**, *114*, 229−236.